# LEAF MARKER SPECTRA IDENTIFICATION BY HYPERSPECTRAL IMAGE ACQUISITION AND VERTEX COMPONENT ANALYSIS

*Julien Marot and Salah Bourennane*

Institut Fresnel/GSM, Aix Marseille Université
D. U. de Saint-Jérôme, av. Normandie Niemen, 13397, Marseille, France
email: julien.marot@fresnel.fr

## ABSTRACT

To monitor biological systems, aside destructive testing which have been developed in chemistry and chromatography, hyperspectral image acquisition and processing exhibit the great advantage of being non-destructive. In this paper, a hyperspectral image acquisition setup is proposed, to get detailed information on the reflectance of leaves. We aim at giving information about the repartition of pigments on a leaf, by proposing a hyperspectral image acquisition setup, and adapting an algebraic method, vertex component analysis, which selects, among a set of input spectra, the marker spectra which best yield all input spectra by linear combination. A matrix inversion yields the contribution of the marker spectra for any spectrum. We acquired the image of leaves and estimated pigment concentrations with the help of a reflectance index.

***Index Terms***— Remote sensing; Hyperspectral imaging; Linear algebra; Feature extraction; Spectrum.

## 1. INTRODUCTION

This paper is concerned with the impact of a technological advance, namely hyperspectral imaging, on environment monitoring. We propose prospects for the adaptation of hyperspectral image (HSI) acquisition and processing to plant growth surveillance. Color images have led to numerous studies, for denoising and segmentation purposes for instance, but a new trend consists in acquiring and exploiting hyperspectral images. A hyperspectral image comes from the observation of a scene at several wavelengths separated by a few nanometers or less. By exploiting a hyperspectral image, it is possible to study a material owing to this principle: each material is characterized by a spectral reflectivity, also called spectral signature. Recent works have shown the interest of hyperspectral data in various fields, including planetology [1] and botany [2]. In this study we focus on hyperspectral imagery applied to non destructive control of plants.

In [2, 3] hyperspectral imagery permits to detect anomalies on sugar beet leaves, and in [4] some indices are calculated to determine, in the leaf, the proportion of pigments such as chlorophyll, carotenoid, and anthocyanin. Chlorophyll indicates the potential productivity of a culture or the biomass of the forest. In [5], through chlorophyll fluorescence visualization, but also by computing a ratio between spectral reflectance values, multispectral imaging permits to evaluate the photosynthetic activity. Carotenoid takes part actively in the good functioning of the plant by protecting it from an excess of light and heat, and also informs about the growing conditions of the vegetation; anthocyanin, takes part to plants coloration, and has an array of health-promoting benefits for the plant itself, but also for human beings when adequately ingested [6]. Anthocyanins form part of a wider family: the phenolic compounds. Some phenolic compounds are produced when a plant reacts to a stress [7]. The importance of these three types of pigments in plant physiology proves the interest to quantify these pigments.

Chemical methods mostly lead to the plant destruction [2, 4], and are labour intensive and time consuming [5]. Hence, multispectral [4] and hyperspectral [2, 5] imaging in narrow spectral bands, are presented as a convincing method to extract information regarding concentrations of specific compounds in plants. To estimate the relative proportion of each pigment in a leaf, usually, indices such as NDVI (normalized difference vegetation index) are used. NDVI is adapted to quantify the proportion of sane vegetation in a remote-sensing context but to our knowledge, it is not meant to distinguish chlorophyll from other pigments and provide its concentration pixel-wise. In [4], hyperspectral imaging techniques are used to identify Arabidopsis mutants with altered leaf pigment status. The authors aim at visualizing individual concentrations and compositional parameters of leaf pigments based on reflectance indices (RIs) developed for Chls a and b, carotenoids and anthocyanins. The interest of studying the phenotypes of plants, through their reflectance spectrum, is emphasized. Their approach based on reflectance indices is very valuable, however, it does not lead to a comprehensive use of the hyperspectral data, because a few wavelengths are selected to compute the RIs. The reflectance values at other wavelengths are not exploited.

Referring to [2], there is a great interest to study a leaf at

high resolution and macroscopic level. Based on their experiments, the authors provide some rules to handle with a hyperspectral acquisition system in the context of nondestructive plant control. They notice that near-range systems are preferable to far-range acquisition systems for the detection of disease symptoms on the leaf or plant scale; that the portion of a signal from a diseased tissue in a mixed signal depends on disease severity [2]. Especially at low disease severities, spectra are based on high percentage from healthy tissue, and only a low portion of symptomatic tissue may cause change in the spectrum [2]. Although this is an issue of great interest, to our knowledge, no method was applied to quantify various types of substances at the local level. Instead of it, in [2] and [3], the SAM (spectral angle mapper) classification method is adapted to distinguish three classes in hyperspectral images containing about 200 bands: 'healthy', 'light mycelium' of powdery mildew, and 'dense mycelium' of powdery mildew. The main limitations of any classification method, and SAM in particular, are as follows: the segmented regions correspond to the dominant reflectance spectrum in these regions. A classification method does not characterize mixtures. In [5], local reflectance values yield the corresponding local plant characteristics: there is no common processing of a set of spectra. Now, we predict that extracting dominant or reference information from a set of spectra is worth considering.

Some pending issues can be drawn from the literature.

In [3], the authors point out that, from a general point of view, "the identification of a disease ... using sensing techniques is still a challenge in vegetation monitoring", and that "interpretation of spectral reflectance data without knowledge on spectral characteristics of leaves and typical symptoms is impossible at present." This point out the lack of reliable "reference" or marker spectra for sake of comparison in a given situation. From this state-of-the-art, it appears that introducing advanced signal processing methods in the context of nondestructive plant analysis would be very valuable for this field. The visual aspect of a leaf is the starting point of our study: zones of a leaf with noteworthy colorations will provide input spectra. Indeed, a hyperspectral camera provides reflectance values at a large number of wavelengths with a high resolution. This permits to go beyond the visual aspect of the leaf and characterize the zones which were selected rigorously, by their corresponding spectrum. We then aim at selecting marker spectra, to study their contribution on the whole leaf.

Our hyperspectral acquisition system is presented in section 2. In section 3 we adapt vertex component analysis. This method selects marker spectra from the set of input spectra. These are the spectra which best yield all other studied spectra by linear combination. By computing a pseudo-inverse, we get the contribution of each marker spectrum in every input spectra extracted from the hyperspectral image. In section 4 we perform hyperspectral image acquisition from two different leaves. Then, we study the pigment content of leaves through their spectral reflectance.

## 2. ACQUISITION CONDITIONS, HYPOTHESES AND OBJECTIVES

Our hyperspectral image acquisition system is composed of an sCMOS VIS-NIR camera containing a linear scanning spectrograph with a sensitivity in the wavelength domain 400-1000 nm, and a spectral resolution 0.6 nm. The viewing angle of the camera is $30°$. The grey level dynamics for each band is 16 bits. For the illumination of the scene, two lamps are used which emit a white light with approximately flat spectrum in the wavelength domain 400-1000 nm. The illumination constraint is then not as harsh as in a fluorescence setup [7]. We also afford a software which is adapted to the camera. The spatial resolution is $8\ 10^{-5}$ m per pixel at the height of the camera, 0.27 m. Referring to [2], a spatial resolution of $2\ 10^{-4}$ m per pixel is optimal to visualize characteristic leaf spots caused by a fungi. Our imaging system provides a resolution of $8\ 10^{-5}$ m per pixel, but we average spectra from a window of size $10 \times 10$ pixels. Therefore the equivalent resolution is $8\ 10^{-4}$ m per pixel. With this equivalent resolution, the amount of pixels with mixed information is significant and it is of great interest to unmix the data resulting from a set of spectra. It is worthwhile noticing that the size of pigment molecules is a few nanometers. Hence, we can assume that there are always several types of pigments which contribute to the spectrum in a given location. Before they are exploited, the images have to be normalized with respect to a white $99\%$ reflecting panel. Then, we select the wavelength region of interest: $400 - 900$ nm.

Our hypotheses are as follows: we consider that spectral pixels of a hyperspectral image are linear combinations of spectra called "endmembers", that we call markers because they are noteworthy. The coefficients of the linear combinations are called "abundances". Referring to plant physiology [4], the markers are related indistinctly to three main pigments: chlorophyll, carotenoid, and an anthocyanin. We aim at estimating the contribution of each marker spectrum anywhere on a leaf. For this, we first adapt the vertex component analysis (VCA) to select the marker spectra; then a matrix inversion yields the mixing coefficients.

## 3. VERTEX COMPONENT ANALYSIS ADAPTED TO MARKER SPECTRA SELECTION

To set the link between algebraic methods and hyperspectral images, an HSI is considered from a mathematical point of view as a multidimensional array, also called "tensor" [8], of order 3 $\mathcal{T} \in \mathbb{R}^{I_1 \times I_2 \times L}$, where $I_1$ is the number of rows, $I_2$ is the number of columns, and $L$ is the number of channels. This image can be flattened as a 2D matrix $\mathbf{T}_3$, along the wavelength mode [8]. The columns of this matrix are the spectral pixels. In the following, we select a subset of $S \leq I_1 I_2$ columns of $\mathbf{T}_3$ and set them column-wise in a matrix $\mathbf{Y}$ of size $L \times S$.

Vertex component analysis of Hyperspectral images is similar to principal component analysis or Gram-Schmidt to reduce the dimensions of the data. This is used in human vision perception and color imaging where 3 primaries are used to represent the data.
Let's consider one column of matrix $\mathbf{Y}$, a spectral pixel denoted by $\mathbf{y}$, which is a vector of size $L \times 1$. The model that we adopt for $\mathbf{y}$ is the linear combination of $p$ endmembers denoted by $\mathbf{x}_i$ ($i = 1, \ldots, p$). Vector $\mathbf{y}$ is expressed as:

$$\mathbf{y} = \mathbf{X} * \mathbf{a} \tag{1}$$

where
$\mathbf{X} = [\mathbf{x}_1, \mathbf{x}_2, \ldots, \mathbf{x}_p]$ and $\mathbf{a} = [a_1, a_2, \ldots, a_p]^T$, where $a_1, a_2, \ldots, a_p$ are the abundances of each endmember.
The abundances $a_k,\ k = 1, \ldots, p$ are such that:

$$0 \leq a_k \leq 1 \tag{2}$$

$$\sum_{k=1}^{p} a_k = 1 \tag{3}$$

Each spectral pixel is considered as a vector in a Euclidean space of dimension $L$. VCA algorithm requires as an input a set of spectral pixels, among which marker spectra must be present. It iteratively projects data onto a direction which is orthogonal to the subspace spanned by the already estimated endmembers. The new endmember signature corresponds to the extreme of the projection. The algorithm iterates until the number of endmembers is exhausted.

In Fig. 1 is represented this Euclidean space, restricted to two bands (two spectral pixel components). As is shown by Fig. 1, because of physical constraints (see Eq. (2) and Eq. (3)) vector $\mathbf{y}$ belong to a simplex [9] whose summits represent the markers. Vector $\mathbf{f}$ bears the direction for data projection. Algorithm 1 details vertex component analysis, which extracts marker spectra.

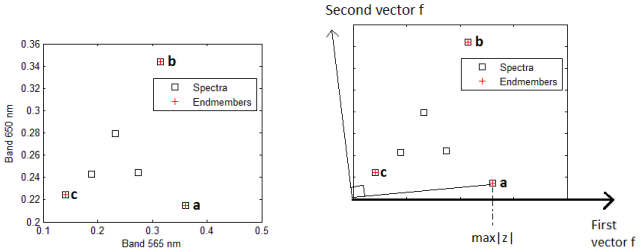


a) b)

**Fig. 1**. a) Mixed spectral data; b) Illustration of the VCA algorithm, including the first two instances of $\mathbf{f}$ and the choice of the first marker by a maximum argument.

In algorithm 1, the following matrices are handled:
$\mathbf{Y} = [\mathbf{y}_1, \mathbf{y}_2, \ldots, \mathbf{y}_S]$ ($S$ is the number of input spectra)

**Algorithm 1** $VCA$

Input: $p$ and $\mathbf{Y} = [\mathbf{y}_1, \mathbf{y}_2, \ldots, \mathbf{y}_S]$
$\hat{\mathbf{X}} = \mathbf{0}$, matrix of marker spectra of size $L \times p$;
Project the data onto a $p$-dimensional subspace:
for all $s = 1, \ldots, S$, $[B]_{:,s} \leftarrow \mathbf{U}^T [Y]_{:,s} - \bar{\mathbf{y}}$ where $\mathbf{U}^T$ is obtained from $\mathbf{Y}$ by PCA,
and $\bar{\mathbf{y}}$ is the mean of vectors $\mathbf{y}_1, \mathbf{y}_2, \ldots, \mathbf{y}_S$.
$c = \underset{s=1,\ldots,S}{\operatorname{argmax}} [B]_{:,s}$
$\mathbf{c} = [c, c, \ldots, c]$ ($\mathbf{c}$ is a $1 \times S$ vector)
$\mathbf{Y} = \begin{bmatrix} \mathbf{B} \\ \mathbf{c} \end{bmatrix}$
$\mathbf{f} = [1, 0, \ldots, 0]^T$ vector of size $L \times 1$
**for** $j \in [1, p]$ **do**
  $\mathbf{z} = \mathbf{f}^T \mathbf{Y}$;
  $k = \underset{s=1,\ldots,S}{\operatorname{argmax}} |z(s)|$
  $[\hat{\mathbf{X}}]_{:,j} = [\mathbf{Y}]_{:,k}$
  generate a vector $\mathbf{f}$ orthonormal to span$([\hat{\mathbf{X}}]_{:,1:j})$
  $\mathbf{f} = \text{orthonormal}([\hat{\mathbf{X}}]_{:,1:j})$
**end for**

$\hat{\mathbf{X}}$ estimated matrix of marker spectra
$[\hat{X}]_{:,j}$ $j^{\text{th}}$ column of $\hat{\mathbf{X}}$
$[\hat{X}]_{:,1:j}$ columns 1 to $j$ of $\hat{\mathbf{X}}$
$[Y]_{:,k}$ $k^{\text{th}}$ column of matrix $\mathbf{Y}$
$|\cdot|$ stands for absolute value.
For $S$ input spectral pixels, there exist $S$ vectors $\mathbf{a}_1, \ldots, \mathbf{a}_S$ whose coefficients are the abundances for each spectral pixel. By grouping all abundance vectors in an abundance matrix $\mathbf{A} = [\mathbf{a}_1, \ldots, \mathbf{a}_S]$, we can express the matrix containing the input spectra as: $\mathbf{Y} = \mathbf{X} * \mathbf{A}$. The estimated abundance matrix $\hat{\mathbf{A}}$ is provided from the estimated marker spectra by the following computation:

$$\hat{\mathbf{A}} = \hat{\mathbf{X}}^{\dagger} * \mathbf{Y} \tag{4}$$

where $(\cdot)^{\dagger}$ stands for pseudo-inverse.
For any observation spectrum $\mathbf{y}_s,\ s = 1, \ldots, S$, the corresponding estimated abundance vector is the $s^{\text{th}}$ column of $\hat{\mathbf{A}}$. From the specifications in [9], when data are projected onto a $p$-dimensional subspace, they should remain nonnegative. We set to 0 all negative values in $\hat{\mathbf{A}}$.

## 4. RESULTS

The plants used in these experiments are grown in a natural environment without using any additive substance, and were naturally watered. As an evaluation criterion, we consider the sum-to-one criterion of the estimated matrix coefficients. The aim of the experiments is twice: we aim at finding the marker spectra which, by linear combination, best yield the six input spectra chosen in each experiment. A higher number could be

chosen, if a larger variety of regions is present on the leaf. We estimate the abundance matrix which permits to reconstruct each input spectrum, as a linear combination of the marker spectra. The number of expected marker spectra is estimated: for all input spectra the reflectance values for two bands $i$ and $j$ are selected, and represented as in Fig. 1. If the correlation coefficient between both sets of reflectance values is larger than 0.9, the number of sources is set to 2; if not, it is set to 3. The acquired HSIs exhibit $L = 777$ bands, downsampled by a factor of 5 to fasten the processing.

### 4.1. Transition between symptomatic and asymptomatic tissues

We consider arabidopsis leaves with symptomatic and asymptomatic regions (see Fig. 2a)). From its color, a location seems to correspond to a purely asymptomatic zone of the leaf. It is denoted by a grey square. The symptomatic regions appear as rather yellow or white. Their color may be due to a lack of chlorophyll and carotenoid and/or to the presence of mycelial colonies. These colonies expand rapidly over the leaf surface. A plant where chlorophyll is lacking is not productive, and a plant which is contaminated should be immediately removed from any set of cultivated plant, so that it does not contaminate its neighbors. Hence the interest of detecting a region whose chlorophyll concentration is below a certain threshold.

The black squares on Fig. 2b), in addition to the grey square, indicate the locations of the selected spectra represented on Fig. 3a). The spectrum corresponding to the grey square is the last column of $\mathbf{Y}$. As shown in Fig. 3b), the spectra are aligned, with a correlation coefficient of 0.999, on a segment delimitated by two summits: the value of the correlation coefficient indicates that among the input spectra, there are two marker spectra (they are emphasized in Fig. 3b) by two crosses), which yield all input spectra by linear combination. We then set $p = 2$ while running VCA algorithm. The estimated mixing matrix $\hat{\mathbf{A}}$ (see Eq. (4)) is as follows:

$$\begin{bmatrix} 0 & 0.2573 & 0.3898 & 0.5578 & 0.7861 & 1 \\ 1 & 0.7427 & 0.6102 & 0.4422 & 0.2139 & 0 \end{bmatrix}$$

The summation of the coefficients of $\hat{\mathbf{A}}$ is always 1, for each column. We get the marker spectra represented on Fig. 3c). We notice that one of them exhibits a relative maximum at 550 nm, which is the distinctive character of chlorophyll. This marker spectrum is then related to chlorophyll, without being the spectrum of either chlorophyll a or b. It results much more reliably from the contribution of carotenoid and chlorophyll because chlorophyll cannot be the single contributor of this spectrum at this observation scale. Owing to the shape of the second marker spectra, we can assume that the production of chlorophyll has stopped in this location. It does not exhibit the characteristic relative maximum at 550 nm. The last column of $\mathbf{Y}$ contains the spectrum associated with the greenest pixel. We notice that, in matrix $\hat{\mathbf{A}}$, the last column exhibits a 1 on the first row. From this, we deduce that the first row of $\hat{\mathbf{A}}$ yields the contribution of the first marker spectrum.

We now look for the chlorophyll concentration at all locations of the input spectra. To this aim, we use reflectance indices. NDVI is well-known and adapted to quantify the proportion of sane vegetation in a region which also comprises soil [10] or fungi [11]. To our knowledge, it is used in remote-sensing contexts at large spatial scales. So, to obtain the chlorophyll concentration at any location, we refer to the reflectance index proposed in [4]: $RI = y_{786}/y_{673} - 1$ where $y_\lambda$ is the reflectance value at wavelength $\lambda$ for the input spectrum $\mathbf{y}$, which yields the chlorophyll concentration $\mathcal{C} = 1.0974\ RI + 0.0219$. Firstly, we apply this method to the greenest region. Indeed, we can expect that the error on the estimated concentration will be the lowest for high chlorophyll concentration values [4]. We obtain $\mathcal{C} = 5.46$ nmol.mg$^{-1}$. Secondly, by multiplying this value by the coefficients in the first row of $\hat{\mathbf{A}}$, we get the chlorophyll concentrations at the six considered regions (in nmol.mg$^{-1}$): 0, 1.41, 2.13, 3.05, 4.29, 5.46. By using matrix $\hat{\mathbf{A}}$, we avoid applying the reflectance index computation to all locations. We notice that the reflectance index in [4] yields an unchanged RI when the two reflectance values of interest are modified by the same multiplicative factor. On the contrary, the proposed method yields matrix $\hat{\mathbf{A}}$ from reflectance values for numerous wavelengths (see Eq. (4)).

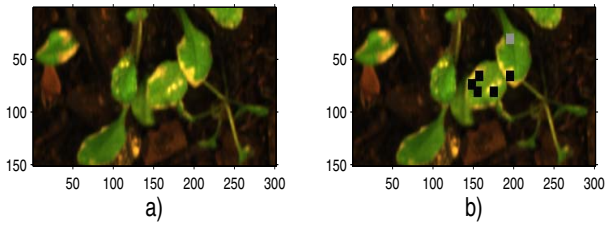


**Fig. 2**. Ill arabidopsis: a) acquired hyperspectral image; b) location of the input spectra.

We expect this method to be more reliable than RI computation, because it uses more non-redundant information.

### 4.2. Case of three marker spectra

We now consider the case where three markers can be selected from the input spectra. We also emphasize the relationship between the number of expected markers and the number of significant pigments. Anthocyanin is a UV-absorbing pigment which protects the leaf from an excess of light and UV-rays. In [12], measurements of *in vivo* chlorophyll fluorescence indicated that the ratio of UV-absorbing screening

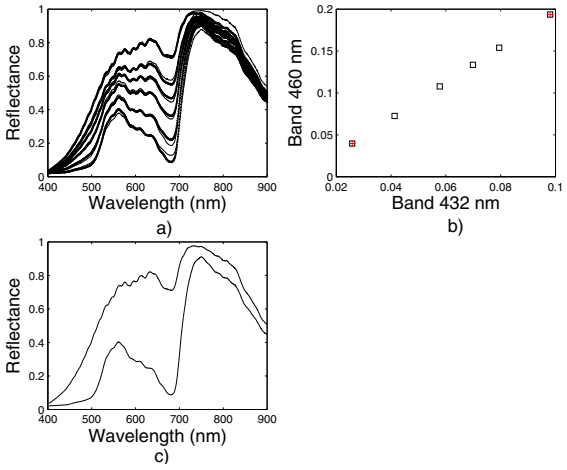


**Fig. 3**. Ill arabidopsis: a) superposition input (-) and reconstructed ($\cdot$) spectra; b) reflectance value at 460 nm vs reflectance value at 432 nm; c) unmixed spectra.

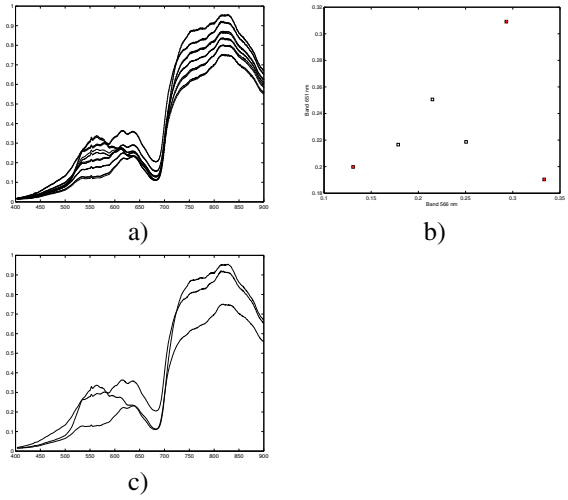


**Fig. 5**. Young leaf: a) superposition input (-) and reconstructed ($\cdot$) spectra ; b) reflectance value at 651 nm vs reflectance value at 566 nm; c) unmixed spectra.

pigments per leaf area increases from the leaf base to the top. This is coherent with the aspect of the young leaf on Fig. 4a), which appears green at the base and red on the borders. We aim at quantifying this evolution in terms of pigment concentration with VCA method, by selecting marker spectra (see the black and white squares in Fig. 4b)). The white square denotes the greenmost location.

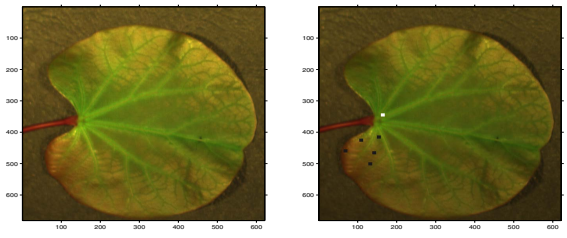


**Fig. 4**. Young leaf: a) acquired hyperspectral image; b) location of the selected spectra.

Fig. 5a) displays the input spectra corresponding to the black squares and the white square in Fig. 4b), as well as the reconstructed spectra. Fig. 5b) represents the reflectance value for each input spectrum at bands 651 nm vs 566 nm. It shows that the input spectra are contained in a simplex with three summits. The correlation coefficient between the two sets of reflectance values is $0.2 < 0.9$, so the number of marker spectra is set to $p = 3$. Fig. 5c) presents the three marker spectra provided by VCA algorithm. They are associated with the red crosses in Fig. 5b)). The estimated mixing matrix (see Eq. (4)) is:

$$\hat{\mathbf{A}} = \begin{bmatrix} 0.7317 & 0.4922 & 0.3674 & 0 & 1 & 0 \\ 0.1625 & 0.4679 & 0.2089 & 1 & 0 & 0 \\ 0.1058 & 0.0399 & 0.4237 & 0 & 0 & 1 \end{bmatrix}$$

One row corresponds to one marker spectrum, and one column to one location in the leaf. The summation of the coefficients of $\mathbf{A}$ for each column is always 1.

Among the marker spectra, one exhibits a relative maximum at 550 nm (see Fig. 5c)). It corresponds to the white square in Fig. 4b) and the last column of $\mathbf{Y}$. This relative maximum is characteristic from chlorophyll and we can, in a first approximation, assert that this marker spectra informs about the repartition of chlorophyll on the leaf surface. The higher the coefficient in the third row of $\hat{\mathbf{A}}$, the higher the chlorophyll content at the corresponding location. For instance, apart from the white square, the location containing most chlorophyll is $\{410, 150\}$ (see column 3 of $\hat{\mathbf{A}}$, exhibiting the coefficient $0.4237$). The second spectrum corresponds to the fifth column of $\hat{\mathbf{A}}$, and to the location $\{454, 55\}$, which exhibits the characteristic red color of anthocyanin. The third spectrum corresponds to the fourth column of $\hat{\mathbf{A}}$, and to location $\{420, 105\}$. It exhibits the characteristic flatness of carotenoid spectrum between 500 and 650 nm. These three spectra are the closest possible to the spectra of chlorophyll, anthocyanin and carotenoid in these acquisition conditions. Similarly to a recent study [4], we aim at getting the concentration of chlorophyll 'a' (whose abundance is known to be generally much higher than chlorophyll 'b') at each location of the leaf with the help of the relevant reflectance index proposed in [4]: $RI = \frac{y_{772-800}}{y_{670-676}} - 1$, which yields the chlorophyll 'a' concentration $\mathcal{C} = 1.0974\, RI + 0.0219$. Contrary to what

is done in [4], we wish to compute RI only at the most reliable location, *i.e.* where the chlorophyll concentration is the highest. First, we compute the RI and the chlorophyll concentration to the greenmost location. We obtain $\mathcal{C} = 6.47$ nmol.mg$^{-1}$. Then, we get an approximation of the concentration at all locations from matrix $\hat{\mathbf{A}}$. By multiplying this value by the coefficients in the third row of $\hat{\mathbf{A}}$, we get the chlorophyll 'a' concentration at the six considered regions (in nmol.mg$^{-1}$): 4.07, 3.59, 4.67, 3.88, 3.80, 6.47. For sake of comparison, although it is generally used in a remote sensing context, we provide NDVI value computed from the spectrum of each location. Here are $NDVI = \frac{(y_{850}-y_{662})}{(y_{850}+y_{662})}$, and the obtained values: 0.60, 0.57, 0.62, 0.58, 0.57, 0.69. In both cases, the rank from most to least concentrated in chlorophyll is 6, 3, 1, 4, 5, 2.

When 750 bands are acquired, the number of rows is 500 and the number of columns 2560, the acquisition time is 40 sec., and the size of the data is 1,8 GB. On a 2-core 3GHz PC running Windows and working with Matlab, opening this image, selecting the leaf of interest, resampling the image to the size $650 \times 650 \times 186$ and processing 6 input spectra to get three marker spectra and the associated abundance coefficients requires 2.5 sec.

## 5. CONCLUSION

This paper concerns an application of hyperspectral imaging: non-destructive plant characterization. For the first time, we provide reliably the contribution of marker spectra to any spectrum extracted from a leaf, by adapting vertex component analysis. Experiments have shown that marker spectra are related to pigments, for instance chlorophyll. With the help of a reflectance index proposed in the literature, we compute the chlorophyll concentration on the location where it is maximum, and we extrapolate the chlorophyll concentration on all considered locations of a leaf, using the mixing matrix derived with VCA. These experiments, performed on two leaves of different type, emphasize the advantages of the proposed method: our hyperspectral imaging setup, associated with vertex component analysis, is a non-destructive method; it exploits the whole spectrum, instead of two reflectance values, as done classically to characterize plants, and provides a general piece of information, namely marker spectra, in addition to a local information such as chlorophyll concentration. We estimate the number of contributing marker spectra, and we select these marker spectra automatically, whatever the acquisition conditions, and independently of any reference database.

## 6. REFERENCES


[1] J.-Ph. Combe et. al., "Analysis of OMEGA/Mars Express data hyperspectral data using a Multiple-Endmember Linear Spectral Unmixing Model (MELSUM): Methodology and first results," *Planetary and Space Science*, vol. 56(7), pp. 951-975, May 2008.

[2] AK. Mahlein et. al, "Hyperspectral Imaging for Small-Scale Analysis of Symptoms Caused by Different Sugar Beet Diseases", *Plant Methods*, vol. 8(3), pp. 1-13, January 2012.

[3] AK. Mahlein et. al, "Recent advances in sensing plant diseases for precision crop protection," *Eur J Plant Pathol*, vol. 133, pp. 197-209, May 2012.

[4] O. Matsuda et. al, "Hyperspectral Imaging Techniques for Rapid Identification of Arabidopsis Mutants with Altered Leaf Pigment Status," *Plant and Cell Physiology Advance Access*, vol. 53(6), pp. 1154-1170, June 2012.

[5] L. Chaerle, R. Valcke, and D. Van Der Straeten, "Imaging techniques in plant physiology and agronomy: from simple to multispectral approaches," *Advances in plant physiology*, vol. 5, pp. 135-155, 2003.

[6] Toufektsian et. al, "Chronic dietary intake of plant-derived anthocyanins protects the rat heart against ischemia-reperfusion injury," *J'l. Nutr.*, vol. 138(4), pp. 747-52, April 2008.

[7] L. Chaerle et al., "Multicolor fluorescence imaging for early detection of the hypersensitive reaction to tobacco mosaic virus," *Journal of Plant physiology*, vol. 164, pp. 253-262, March 2007.

[8] D. Muti, S. Bourennane and J. Marot, "Lower-Rank Tensor Approximation and Multiway Filtering," *SIAM Journal on Matrix Analysis and Applications (SIMAX)*, vol. 30(3), pp. 1172-1204, September 2008.

[9] JMP. Nascimento, JMB. Dias, "Vertex component analysis: a fast algorithm to unmix hyperspectral data," *IEEE TGRS*, vol. 43(4), pp. 898-910, April 2005.

[10] Zha, Y., Gao, J., Ni, S., Liu, Y., Jiang, J., & Wei, Y. (2003). A spectral reflectance-based approach to quantification of grassland cover from Landsat TM imagery. *Remote Sensing of Environment*, 87, 371-375.

[11] Moshou, D., Bravo, C., Oberti, R., West, J.S., Ramon, H., Vougioukas, S., & Bochtis, D. (2011). Intelligent multi-sensor system for the detection and treatment of fungal diseases in arable crops. *Biosystems Engineering*, 108(4), 311-321.

[12] H. Wagner, M. Gilbert, C. Wilhelm, "Longitudinal leaf gradients of UV-absorbing screening pigments in barley (Hordeum vulgare)," *Physiol Plant.*, vol. 117(3), pp. 383-391, March 2003.